Investigation of the properties of reactive MgO-based cements and their effect on performance

Mi, Tangwei; Yang, En Hua; Unluer, Cise

Published in:
Cement and Concrete Composites

DOI:
10.1016/j.cemconcomp.2023.104984

Publication date:
2023

Cement and Concrete Composites 138 (2023) 104984

Contents lists available at ScienceDirect

Cement and Concrete Composites

journal homepage: www.elsevier.com/locate/cemconcomp

Investigation of the properties of reactive MgO-based cements and their effect on performance

Tangwei Mi [a], En-Hua Yang [a], Cise Unluer [b,*]

[a] School of Civil and Environmental Engineering, Nanyang Technological University, 50 Nanyang Avenue, 639798, Singapore
[b] Department of Mechanical, Aerospace and Civil Engineering, University of Manchester, M13 9PL, Manchester, United Kingdom

ARTICLE INFO

Keywords:
Reactive MgO-Based cement
MgO
Carbonation
Hydration
Compressive strength
Pearson correlation coefficient

ABSTRACT

Reactive MgO cement (RMC) is a promising alternative cementitious material benefiting from a relatively low calcination temperature during its production and strength development in concrete formulations linked with its CO_2 sequestering capacity. One of the main challenges with RMC is the variations in its performance in line with the significant differences observed in the properties of the main phase, MgO. To identify and analyze the effects of these properties on the performance of RMC, this study presents a detailed characterization of 9 commercial RMC powders from different sources and precursors and an investigation of their performance in terms of reaction mechanisms and strength development. The results showed that the progress of hydration was highly dependent on the reactivity of RMC, whilst the early stages of the reaction were influenced by the purity. Additionally, agglomeration ratio revealed a strong correlation with the strength after 7 days of carbonation curing and 28 days of hydration. Finally, a regression analysis was employed to propose a model for the prediction of strength based on the initial properties of the RMC powder. The results emerging from this study can serve as a guideline for the selection of most suitable RMC-based binders for various building applications.

1. Introduction

Reactive MgO cement (RMC) is investigated as an alternative binder due to its several technical advantages over ordinary Portland cement (OPC) such as its capability of gaining strength by reacting with CO_2, as well as the relatively low calcination temperatures required during its production [1–3]. MgO is mainly sourced from natural minerals and is classified as light-burnt/reactive (700–1000 °C), hard-burnt (1000–1400 °C) and dead-burnt (1400–2000 °C), based on the calcination temperature. Among those, the light-burnt MgO is the most reactive, which is the main phase present in RMC.

One of the main challenges with the use of RMC is the significant variations in the physical and chemical properties of commercial MgO, which is mainly attributed to the differences in the precursors (i.e. composition and physical properties) and production processes (i.e. calcination conditions) [4–6]. In particular, the discrepancies in the major properties of MgO powders, such as chemical composition, reactivity and specific surface area (SSA), can have considerable effects on the performance of RMC as a binder [7,8]. As can be seen in Fig. 1, notable differences in the strength of RMC-based paste and concrete samples were reported in the literature. Although variations in strength could have been caused by the other factors, such as aggregate ratio and curing conditions (i.e. in most cases involving carbonation), differences can still be observed even with comparable mix designs and curing conditions [9,10]. To employ RMC as binder in different building components, selection of suitable MgO powders is necessary. This becomes even more crucial when a high mechanical performance is required. Therefore, there is a need to understand the parameters controlling the performance of MgO and establish correlations between different parameters to optimize the use of this binder in an efficient manner.

Based on their reactivity, commercial MgO powders can be classified as high, medium, and low reactivity [4]. Previous studies reported that the SSA and reactivity could determine the hydration rate of RMC [11]. However, there is a gap in the literature on the effect of reactivity and SSA of RMC on strength development. Apart from SSA and reactivity, the purity of RMC was also reported to affect its hydration and performance [12]. In relation with purity, the amount of MgO available for reaction is one of the main factors that determine the degree of reaction. Alternatively, the chemical reactivity and other physical properties such as SSA and agglomeration degree play a key role in the reaction rate [13]. Although differences in the performance of RMC mixes prepared and

* Corresponding author.
E-mail address: cise.unluer@manchester.ac.uk (C. Unluer).

https://doi.org/10.1016/j.cemconcomp.2023.104984
Received 1 July 2022; Received in revised form 2 February 2023; Accepted 9 February 2023
Available online 11 February 2023

cured under similar conditions are speculated to be associated with the properties of RMC powders, the correlation between these properties and strength development has not been clearly established until now.

Similar to other binder systems, factors like mix design and curing conditions are influential in the performance of RMC-based mixes and need to be kept constant in order to isolate the influence of RMC properties on reaction mechanisms and performance. For example, while the results reported in data sets 2–4 (Fig. 1 (a)) were obtained under the same curing conditions (10% CO_2) as well as water (w/b = 0.60) and binder (MgO content = 92%) contents, the use of different proportions of aggregates in these formulations contributed to the variations in strength. Therefore, the variations in these key parameters across different studies make it challenging to isolate the effect of the properties of RMC on the performance of RMC-based mixes by only relying on the results presented in the literature.

Identification of the properties of RMC that lead to enhanced performance and their optimization play a key role in the large-scale use of RMC as a binder in different building applications. While various studies reported the strength of RMC-based samples at different ages [10, 14–18], a detailed characterization of the binder was not presented. Alternatively, studies that performed some characterization of RMC did not look into the strength development of these powders [4]. Therefore, this study aims to fill this gap and establish a link between RMC properties and mechanical performance to enable the widespread use of RMC. With this goal in mind, this study involves a detailed investigation of the effects of various binder properties including MgO content, SSA, chemical reactivity and agglomeration ratio, on the performance of RMC via the assessment of its hydration mechanism and strength development at different ages.

To enable their direct comparison, 9 commercial RMC powders with different precursor and production conditions were characterized and investigated. To facilitate a fair comparison, the properties of these RMC powders were evaluated under the exact same conditions, without any variations in experimental conditions. In addition to the characterization of their properties, each RMC powder was used as a binder in the preparation concrete samples for further evaluation. The obtained results revealed the roles different RMC properties played in reaction mechanisms and performance and enabled the establishment of correlations between the binder properties and sample performance. Corresponding equations were proposed to predict the strength of RMC concrete samples based on the properties of RMC. The outcomes of this study can provide a guideline for researchers and practitioners interested in using RMC as a binder within the built environment.

2. Materials and methodology

2.1. Materials

Nine commercial RMCs were investigated in the current study. Among them, seven were produced through the dry-route via calcination and the other two were chemically synthesized through the wet-route. Their sources and chemical compositions are summarized in Table 1, and the corresponding appearance are presented in Fig. S1. The information regarding the chemical composition and loss of ignition (LOI) was obtained from the suppliers for reference purposes only. Due to the differences in various batches as well as storage conditions and duration, the actual properties of these nine commercial RMCs may vary from those presented in Table 1. In particular, agglomeration of MgO powders supplied from Australia (AU-97 and AU-90) was observed, potentially due to improper packaging and storage. These two RMCs were included in the study to investigate the effect of moisture and carbonation damage as these materials have been stored in different environments until analysis. Additionally, the chemically synthesized RMCs investigated in this study, CNSH-99 and CNSD-99, were selected due to their extremely high purity (i.e. potentially resulting in better performance) and comparable cost to the other RMCs, as listed in Table 1. Saturated surface dry (SSD) gravel with a particle size of 6.3–9.5 mm was used to form the aggregate profile in the preparation of RMC-based concrete specimens.

2.2. Properties

2.2.1. Purity

The purity of the RMCs was determined by X-ray diffraction (XRD), and the results were verified by Thermogravimetric analysis (TGA). XRD was recorded by Bruker D8 Advance using Cu-K_α radiation (40 kV, 40 mA) with a scanning rate of 0.04° 2θ/step from 5° to 80° (2θ). Phase quantification was performed via the Rietveld refinement software TOPAS 5.0, with fundamental parameter approach [20]. This analysis involved only the crystalline phases for ease of calculation. TGA was performed by a PerkinElmer TGA 4000 equipment from 30 to 900 °C, with a heating rate of 10 °C/min under nitrogen flow. To quantify the amount of mass loss at each decomposition process, derivative thermogravimetric (DTG) curves were deconvoluted according to the Gaussian area deconvolution method using Origin, which revealed the range corresponding to the decomposition process.

2.2.2. Specific surface area (SSA)

The SSA was calculated by using the Brunauer, Emmett and Teller (BET) approach. A BET Surface Area and Pore Size Analyzer,

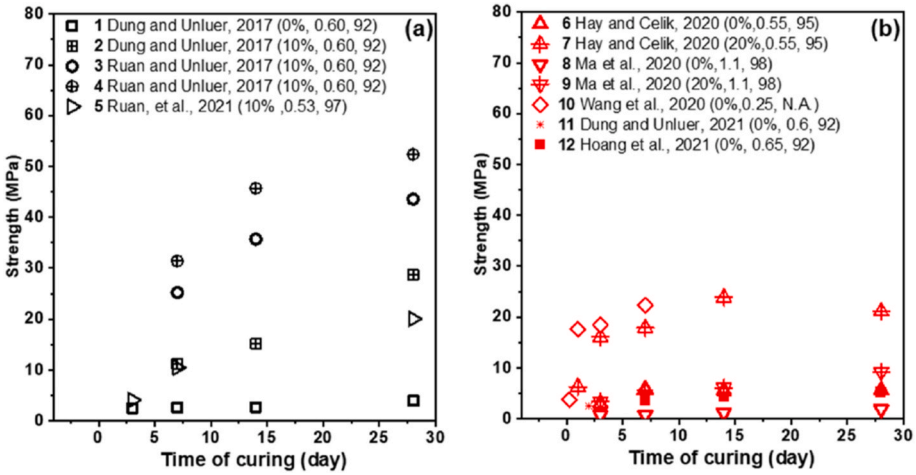

Fig. 1. Strength values of RMC-based (a) concrete and (b) pastes reported in the literature [9,10,14–19].

Table 1
The source and chemical compositions of nine commercial RMCs.

No.		Label	Supplier	Mining source	Chemical composition (%)					LOI (≤)	Price
					MgO (≥)	CaO (≤)	Fe_2O_3 (≤)	SiO_2 (≤)	Al_2O_3 (≤)		(SGD/kg)
Calcination of magnesite	**1**	UKCN-90	RBH, UK	CN	90.7	1.9	0.6	4.4	0.4	2.0	10
	2	UKNK-92	RBH, UK	NK	92.7	1.8	0.8	2.3	–	2.1	10
	3	AU-97	IS, SG	AU	97.0	1.3	0.2	1.3	0.2	2.5	5
	4	AU-90	IS, SG	AU	90.0	5.0	0.7	5.0	0.7	15.0	4
	5	CNSD-92	LCTM, CN	SD, CN	92.7	1.7	0.8	2.3	–	2.5	1.6
	6	CNLN-92	LCTM, CN	LN, CN	92.5	1.8	0.4	3.2	–	–	0.4
	7	CNSH-85	SYCC, CN	LN, CN	85.0	1.5	–	–	–	–	3.2
Chemical synthesis	**8**	CNSH-99	SYCC, CN	–	99.0	0.5	–	–	–	–	4
	9	CNSD-99	SYCC, CN	–	99.2	0.1	0.0	0.1	–	–	5.2

UK: United Kingdom; **CN**: China; **SG**: Singapore; **NK**: North Korea; **AU**: Australia; **SD**: Shandong province in China; **LN**: Liaoning province in China; **SH**: Shanghai, China; **RBH:** Richard Baker Harrison Ltd; **IS:** International Scientific (Pte) Ltd; **SYCC:** Shanghai Yuanjiang Chemicals Co. Ltd; **LCTM:** Lingshou County Teyuan Minerals Processing Plant; **LOI:** Loss on Ignition.
Note: The label of each RMC represents the location of its factory, source of raw materials and minimum purity provided by the supplier (i.e. factory and raw materials of AU-97 and AU-90 are both in Australia, whereas IS (SG) is only a reseller).

manufactured by QUADRASORB evo™, was employed to measure the quantity of nitrogen gas absorbed onto and desorbed from the RMC powders. Prior to each measurement, the gases were removed in a vacuum condition at 80 °C. After degassing for 24 h, nitrogen gas was injected and the SSA was calculated.

2.2.3. Chemical reactivity

To determine the reactivity of each RMC in line with the chemical reaction shown in Equation (1), the time required for 1.5 g of RMC to neutralize 60 ml of 0.25 M acetic acid was recorded by observing the change in color. Phenolphthalein solution (1% in ethanol) was used as a pH indicator.

$$2H^+ + MgO = Mg^{2+} + H_2O \quad (1)$$

2.2.4. Agglomeration ratio (AR)

Agglomeration ratio (AR) is the ratio between the primary particle size and crystallite size, which can be calculated based on the BET and XRD results, respectively. To estimate the crystallite size (G_{XRD}), Scherrer equation was employed, as shown in Equation (2), where k is a constant (0.94 in this case), λ is the wavelength of x-ray radiation (Cu-K_α = 0.1541 nm), β is the full width at half maximum (FWHM) of the most intense peak at 42.93° and θ is the Bragg's or diffraction angle [7].

$$G_{XRD} = k\lambda/\beta \bullet \cos\theta \quad (2)$$

The primary particle size (G_{BET}) of each powder was calculated by following Equation (3), where F is a particle-size factor, ρ is the theoretical density of MgO (3.595 g/cm^3) [4,21] and S is the specific surface area [4]. As MgO is generally composed of cubic particles, F was assumed as 6, in line with the approach adopted in Jin and Al-Tabbaa [4] and Itatani et al. [21].

$$G_{BET} = 1000F/\rho S \quad (3)$$

Consequently, AR was derived by calculating G_{BET}/G_{XRD}. As a primary particle may consist of several crystallites, the value of AR represents the degree of particle agglomeration.

2.2.5. Microstructure

The microstructure of the reactive MgO were characterized by Zeiss Evo 50 microscope. Energy-dispersive X-ray (EDX) was employed to identify the elemental distribution with a resolution of 256 × 192 pixels. To eliminate the charging phenomenon, the samples were coated with gold under 10 mA for 30s. Vacuum dried samples were mounted onto sample stage by using double-sided adhesive carbon tape.

2.3. Performance

2.3.1. Heat of hydration

The heat of hydration of each RMC was investigated by an I-Cal 8000 high precision calorimeter, in accordance with ASTM C1702-15a [22]. 40 g RMC powder and 20 g deionized water (increased to 24 g water for CNSH-85 and 40 g water for CNSH-99 to match their water demands) were heated at 30 °C for 24 h to ensure that all materials started with the same initial temperature. Afterwards, the RMC powders and water were mixed for around 15 s and immediately placed into the isothermal calorimeter channel for analysis.

2.3.2. Compressive strength

The compressive strength of RMC-based concrete specimens was assessed via the assessment of 50 mm cubes in triplicates at 3, 7 and 28 days, in accordance with ASTM C109 [23]. A Toni Technik Baustoffprüfsysteme machine was employed with a loading rate of 55 kN/min. The prepared concrete mixes were composed of 40% binder and 60% aggregates with a water-to-binder (w/b) ratio of 0.5, apart from CNSH-85 (w/b = 0.6) and CNSH-99 (w/b = 1), whose water contents had to be increased to achieve a comparable workability with the other RMC mixes. The prepared concrete specimens were subjected to two different curing regimes: (i) Carbonation curing (28 ± 2 °C, 80 ± 5% relative humidity (RH) and 10% CO_2) and (ii) ambient curing (28 ± 2 °C, 80 ± 5% RH and ambient CO_2), for up to 28 days.

3. Results and discussion

3.1. Properties

3.1.1. MgO contents

The TGA -DTG results of the nine RMC samples are shown in Fig. 2. Three major decomposition stages were determined as: (i) 50–200 °C for the dehydration of water bonded to hydrated magnesium carbonates (HMCs), (ii) 200–450 °C for the dehydration of HMCs and decomposition of brucite ($MgOH_2$) [18,24]; (iii) > 450 °C for the decarbonation of carbonate phases (e.g. HMCs and $MgCO_3$) [18,25]. The mass loss recorded at each of these three stages was plotted in Fig. 3. It can be seen that the mass loss in the 50–200 °C range was less than 1% for almost all samples. In particular, there was almost no mass loss for CNLN-92 and CNSD-99. In the range from 200 °C to 450 °C, AU-97 and AU-90 samples exhibited a significant mass loss of 16.73% and 14.32%, respectively. This indicates a high amount of brucite formation within these samples, probably due to the improper storage conditions, leading to the hydration of MgO when exposed to the moisture in the air [4,26]. Other RMC samples exhibited a mass loss of 5% or less. At temperatures >450 °C, CNSD-92 revealed a high mass loss (22%), indicating its high carbonate

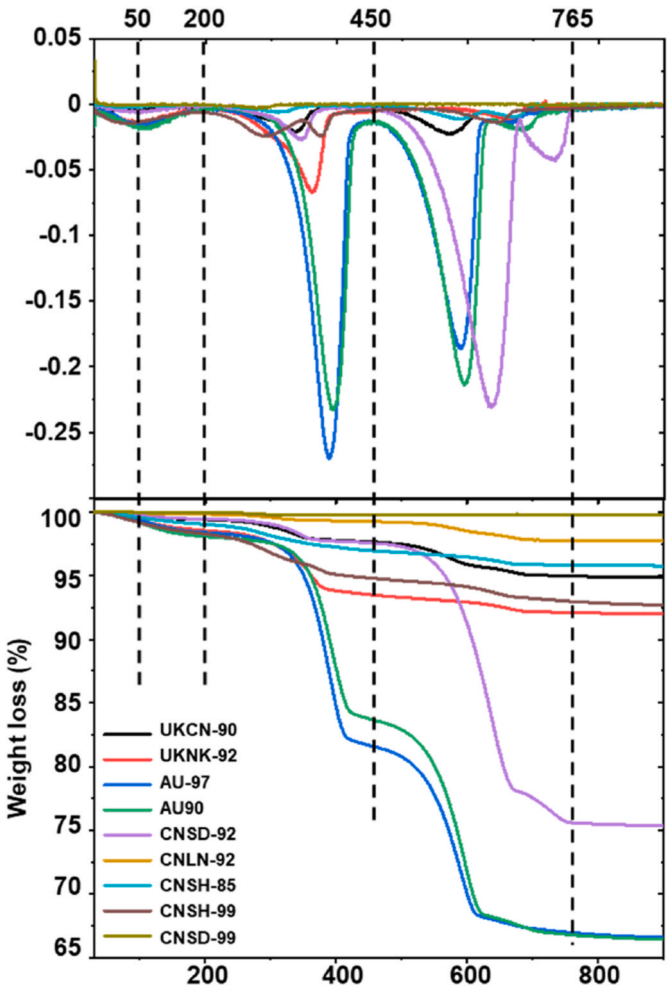

Fig. 2. TGA and DTG curves of the nine commercial RMCs.

content, which was partially attributed to the low calcination temperature (750 °C) used during its production [27]. Samples AU-97 and AU-90 also resulted in high mass losses at this temperature range (14.72% and 16.98%, respectively), suggesting their potential carbonation due to improper storage and the incomplete decomposition of the parent material. Overall, the TGA results revealed significant differences in the compositions of RMC samples.

XRD patterns of the RMC samples are shown in Fig. 4. As can be seen, strong peaks at 42.8° and 62.2° 2θ, indicating the presence of MgO as the major compound [9,28], were observed in all RMC samples. Furthermore, peaks at 32.7° and 53.8° 2θ, referring to magnesite, were also observed in all RMC samples, demonstrating the incomplete decomposition of the parent minerals [9]. The chemically synthesized RMC samples (CNSH-99 and CNSD-99) also contained magnesite, which might be sourced from the synthesis process [29]. The XRD patterns of AU-97 and AU-90 presented strong peaks at 18.4° 2θ, implying the existence of large amounts of brucite [30], consistent with the TGA results. Additionally, the peaks at 9.4°, 26.6° and 31.0° 2θ in CNSD-92 sample suggested the presence of hydromagnesite [9], whilst the peak at 23.1° 2θ in CNLN-92 could be assigned to nesquehonite [16,31,32], which was different from the amorphous SiO_2 hump observed in CNSH-85, CNSH-99 and CNSD-99.

Fig. 5 lists the quantities of minerals in the nine commercial RMC samples. As can be seen, MgO was the major phase in most samples with a content of 90% and above, apart from AU-97, AU-90 and CNSD-92, which was in agreement with the TGA results. AU-97 and AU90 had the highest brucite contents of 42.6% and 33.1%, respectively; while others contained much less brucite (≤6%). In terms of carbonates, AU-97, AU-90 and CNSD-92 showed relatively high contents of carbonate compounds (e.g. magnesite, hydromagnesite and nesquehonite), measured as 37.5%, 42.7% and 57.8%, respectively. Alternatively, CNSD-92 and CNLN-92 revealed hydromagnesite and nesquehonite contents of 13.9% and 3.5%, respectively. The presence of brucite and HMC phases were an indication that RMC samples experienced different degrees of hydration and carbonation, even before the analysis. These findings clearly highlighted the need for the proper storage for RMC powders under controlled humidity and CO_2 conditions.

3.1.2. Specific surface area (SSA)

The SSA results, determined by BET, are shown in Fig. 6. Generally, the SSA of the nine RMC samples was within the range reported in the literature [4]. CNSH-99 revealed the largest SSA of 86.9 m^2/g, followed by CNSH-85 (33.5 m^2/g). Others had SSAs in the range of 4–20 m^2/g, amongst which, CNLN-92 and CNSD-99 demonstrated the lowest values of 5.8 and 4.4 m^2/g, respectively. The low SSA of CNLN-92 could be attributed to the relatively high calcination temperature used during its production [6]. Considering that SSA indicates the available surface of particles to reactants, samples with higher SSA values could be expected to have higher reactivities [33]. In the current study, CNSH-99 and CNSH-85 had the largest SSA, potentially suggesting high reaction rates. In contrast, CNLN-92 and CNSD-99 were expected to have lower reaction rates due to their relatively low SSA values.

3.1.3. Chemical reactivity

The reactivities of all RMC samples, measured by the time required to

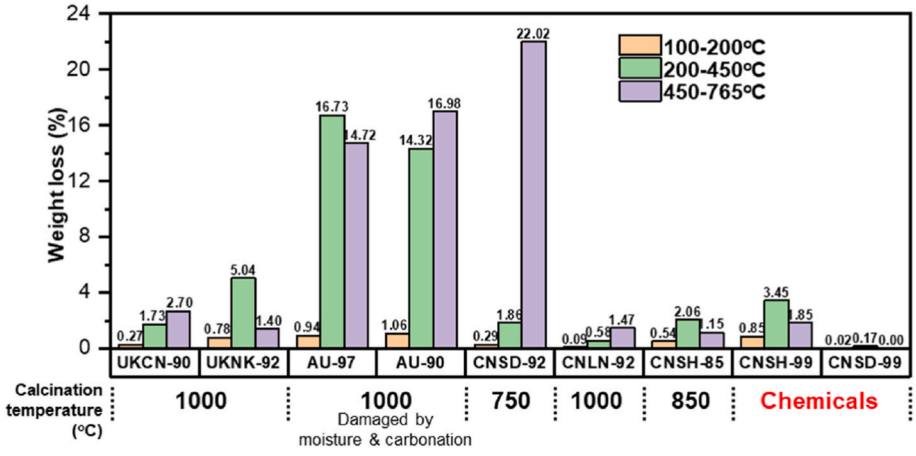

Fig. 3. Mass loss observed in the nine commercial RMCs.

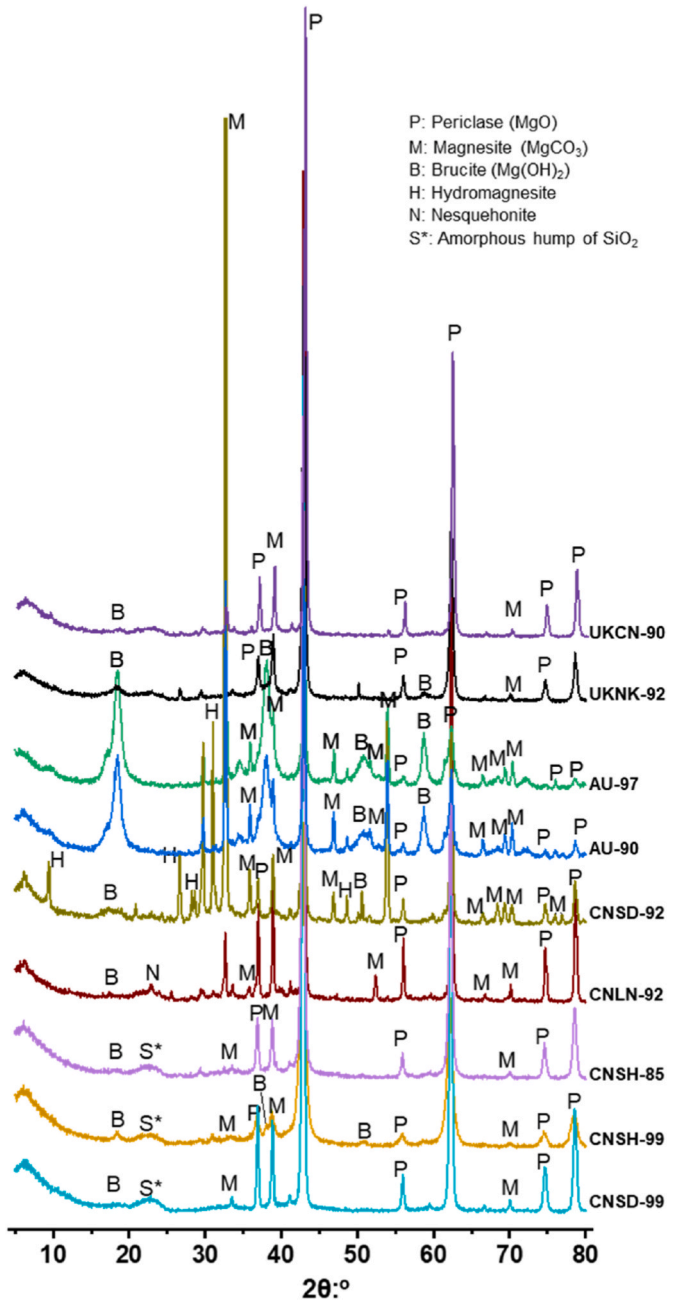

Fig. 4. XRD patterns of the nine commercial RMCs.

neutralize acetic acid solution, are depicted in Fig. 7. The time consumed by different samples varied significantly, ranging from 9 s (i.e. highest reactivity) to 101.7 s (i.e. lowest reactivity). The relatively small standard deviations suggested the reliability and repeatability of the results. CNSH-99 exhibited the highest reactivity, which could be attributed to its very high SSA, as shown in Fig. 6. The lowest reactivity (101.7 s) was observed for CNLN-92, which possessed the second lowest SSA (5.8 m^2/g). CNSD-99, RMC with the lowest SSA (4.4 m^2/g), only took 63 s to achieve neutralization. This phenomenon was partially caused by the slightly higher MgO content of CNSD-99, as reported in Fig. 5. Furthermore, the variations in the microstructures of these RMC powders could also play a role in their reactivities [34].

On the other hand, while CNSD-92 and AU-90 had comparable SSAs (Fig. 6) and similar MgO contents (Fig. 5), the time required for the neutralization of CNSD-92 was around two times that of AU-90. This may be attributed to the high $Mg(OH)_2$ content in AU-90, which dissolves and releases OH^-, thereby shortening the neutralize time. As a result, the results generated by the acid in evaluating the reactivity of RMC may not be very meaningful in the presence of relatively high $Mg(OH)_2$ contents in RMCs.

3.1.4. Agglomeration ratio (AR)

The primary particle size (G_{BET}) and crystallite size (G_{XRD}), calculated based on the BET and XRD results, are listed in Table 2. The agglomeration ratios (AR), derived by G_{BET}/G_{XRD}, indicate the amount of crystallites contained in a primary particle [21]. Among the RMCs produced via the dry-route, CNLN-92 showed a relatively highest agglomeration degree with an AR of 7.2, but the lowest SSA and reactivity (Figs. 6 and 7). In contrast, CNSH-85 possessed the lowest AR of 2, accompanied with the highest SSA and reactivity. These findings were in line with those reported in the literature [4], suggesting a direct correlation amongst AR, SSA and reactivity.

AR of chemically synthesized CNSH-99 was 1.6, which was comparable to that reported in the literature [4]. However, chemically synthesized CNSD-99 revealed a very high AR value of 12.7, which could be highly related to its production process, usually observed in the absence of anti-agglomeration treatment [35]. As agglomeration was usually caused by capillary pressure or surface tension, anti-agglomeration treatment involved minimizing these effects (e.g. increased surface wetting by organic groups) [35]. Overall, the agglomeration degree of the nine commercial RMCs varied significantly, revealing clear differences depending on the production process of the RMCs.

3.1.5. Microstructure

The microstructures of the nine commercial RMCs are shown in Fig. 8. Each sample revealed significantly different microstructures in line with the variations in their particle size, shape and homogeneity, which can affect their performance as a binder. In particular, the variations in the density and agglomeration of RMCs were highlighted in Fig. 8.

Samples UKCN-90 and UKNK-92 were mainly composed of dense MgO particles with grain size less than 100 nm, based on their SEM images [28]. On the contrary, extensive $Mg(OH)_2$ was observed in AU-97 and AU-90 [36,37], which is consistent with their TGA and XRD results. Two distinct morphologies were observed in CNSD-92 and CNLN-92, both dominated by MgO particles with a grain size of around 100–200 nm and a secondary carbonate phase [18,38,39], in line with the XRD results. The morphologies of CNSH-85 and CNSH-99 were more homogenous, consisting of evenly distributed MgO particles. CNSH-85 and CNSH-99 possessed looser microstructures when compared to UKCN-90 and UKNK-92, which could have contributed to their higher SSA. It is worth noting that a certain degree of agglomeration was observed in CNSH-85, resulting in a lower SSA than CNSH-99. Among the nine RMCs, CNSD-99 revealed a microstructure composed of particles that agglomerated into larger volumes. Due to the unique morphology of CNSD-99, EDX was used to evaluate its chemical composition locally. The composition of this sample confirmed by EDX results shown in Fig. S2, mainly included Mg and O. The unique morphology of MgO present within this sample could explain its high AR value.

Some samples experienced mild charging, as can be seen in some images in Fig. 8, which was attributed to their less conductive nature [40]. Though samples were coated by conductive gold, the variation of the properties of RMCs still induced different degrees of charging.

3.2. Correlation among different properties

Fig. 9 shows a strong linear correlation between the chemical reactivity (i.e. the time consumed for neutralization) and SSA of each sample. Reactivity was expressed as reciprocal of as it is inversely related to the neutralization time. The results revealed a direct linear relationship between reactivity and SSA, with an r^2 value of 0.88.

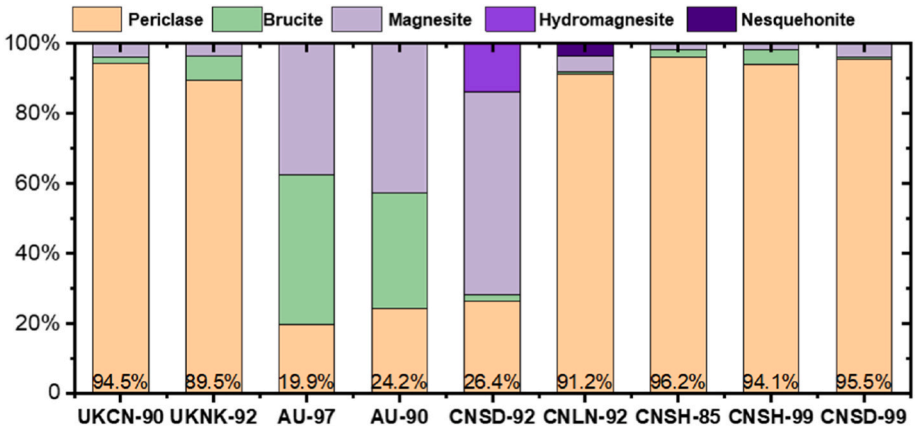

Fig. 5. Periclase (MgO), brucite ($Mg(OH)_2$) and carbonate contents of the nine commercial RMCs.

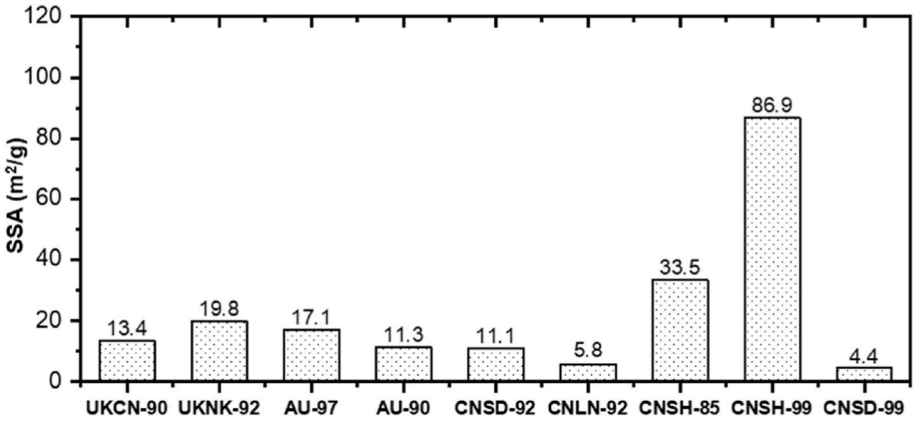

Fig. 6. SSA of the nine commercial RMCs.

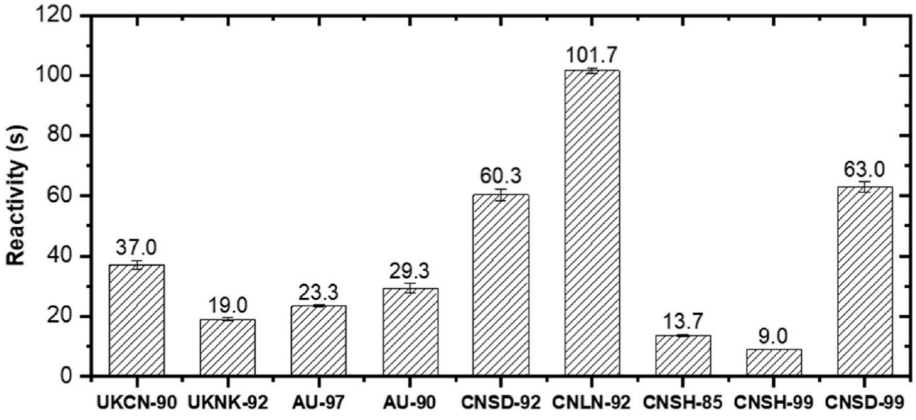

Fig. 7. Chemical reactivities of the nine commercial RMCs.

Fig. 10 presents the correlation of AR with SSA and reactivity. It was reported that the lower the AR value, the higher the reactivity of MgO powder was since the less agglomerated MgO would need to break apart for hydration [4]. While the relationship between SSA and AR of MgO has not been discussed in the literature in detail until now, both SSA and reactivity illustrated inverse proportionality with AR in Fig. 10, showing a considerable drop in SSA and reactivity with an increase in AR when it was below 4. Alternatively, when the AR value was above 4, SSA and reactivity gradually decreased with the further increase of AR, albeit at a significantly lower rate. The coefficients of the inverse curves for each relationship were determined by inverse curve fitting, as presented in Fig. 10. On the other hand, no obvious relationships were observed between the purity (i.e. MgO content) of each sample against the other properties.

3.3. Performance

3.3.1. Heat of hydration

Heat release is linked with the dissolution and hydration of the MgO via its reaction with water to form $Mg(OH)_2$ [41]. The rate of this reaction is dependent on the reactivity of the RMC [34]. Fig. 11 shows the heat flow of the nine RMC samples during the first 72 h of hydration. All

Table 2
Textural properties and crystallite sizes of the nine commercial RMCs.

Label	SSA (m^2/g)	G_{BET}	FWHM (β)	G_{XRD}	AR, G_{BET}/G_{XRD}
UKCN-90	13.437	124.2	0.22916	37.2	3.3
UKNK-92	19.776	84.4	0.31199	27.4	3.1
AU-97	17.098	97.6	0.25296	33.7	2.9
AU-90	11.311	147.6	0.26433	32.3	4.6
CNSD-92	11.058	150.9	0.24787	34.4	4.4
CNLN-92	5.754	290.1	0.21109	40.4	7.2
CNSH-85	33.451	49.9	0.33755	25.3	2.0
CNSH-99	86.945	19.2	0.72444	11.8	1.6
CNSD-99	4.404	379.0	0.28707	29.7	12.7

samples revealed their first peaks within 2 h, corresponding to the initial dissolution of MgO. However, the heat flow rate at the initial stage of the nine RMCs was very different, ranging from 1.1 to 162.8 mW/g. CNSH-85 and CNSH-99 showed rapid initial heat flow rates, aligned with their relatively high reactivities. In contrast, CNLN-92 exhibited the lowest heat flow rate of 1.1 mW/g, in line with its lowest reactivity. The heat flow curves of CNSD-92 and CNSD-99 possessed boarder peaks, which could be attributed to their similarly low reactivities and SSAs. A similar observation was reported in the literature, showing that decreased hydration rate could be reflected as a broad hydration peak, which was in alignment with lower reactivity and SSAs in MgO samples [42,43].

After the first peak, the heat flow of most RMC samples started to decline due to the initial precipitation of hydrates on the unreacted MgO surfaces, which prevented further dissolution and therefore slowed down the hydration reaction [42,44]. CNSH-85, CNSH-99, UKNK-92 and AU-97 samples revealed single sharp hydration peaks, which could be related to their relatively high reactivities [43]. In contrast, CNSD-92 and CNSD-99 samples demonstrated single board peaks, owing to their low reactivities [43]. The other three samples exhibited a second hydration peak between 5.1 and 28.5 h, which was labeled in red in Fig. 11. When all the samples were compared, the role of reactivity in the hydration mechanism of RMC samples was observed, revealing three types of hydration behavior: (i) A single sharp hydration peak; (ii) a single board peak; and (iii) two separate peaks.

Fig. S3 illustrates the cumulative heat of the nine RMC samples during the first 72 h. CNSH-85 and CNSH-99 samples released more heat in the initial stage, in line with their high reactivities. As hydration proceeded, CNSH-85 maintained the highest heat released until 64.5 h, which was then surpassed by CNSD-99. On the contrary, CNLN-92 exhibited the lowest cumulative heat initially, aligned with its lowest reactivity. This was followed by an almost linear increase until the end of 72 h, indicating the constant hydration rate of CNLN-92. The linear increase of cumulative heat observed in CNSD-99 and CNLN-92 samples was an indication of the continuation of the hydration reaction within the first three days. When compared with the others, these samples had the lowest reactivities, slowing down the initial reaction and the associated formation of the hydroxide film. Both AU-97 and AU-90 samples revealed a low heat release at all times, which was correlated with their

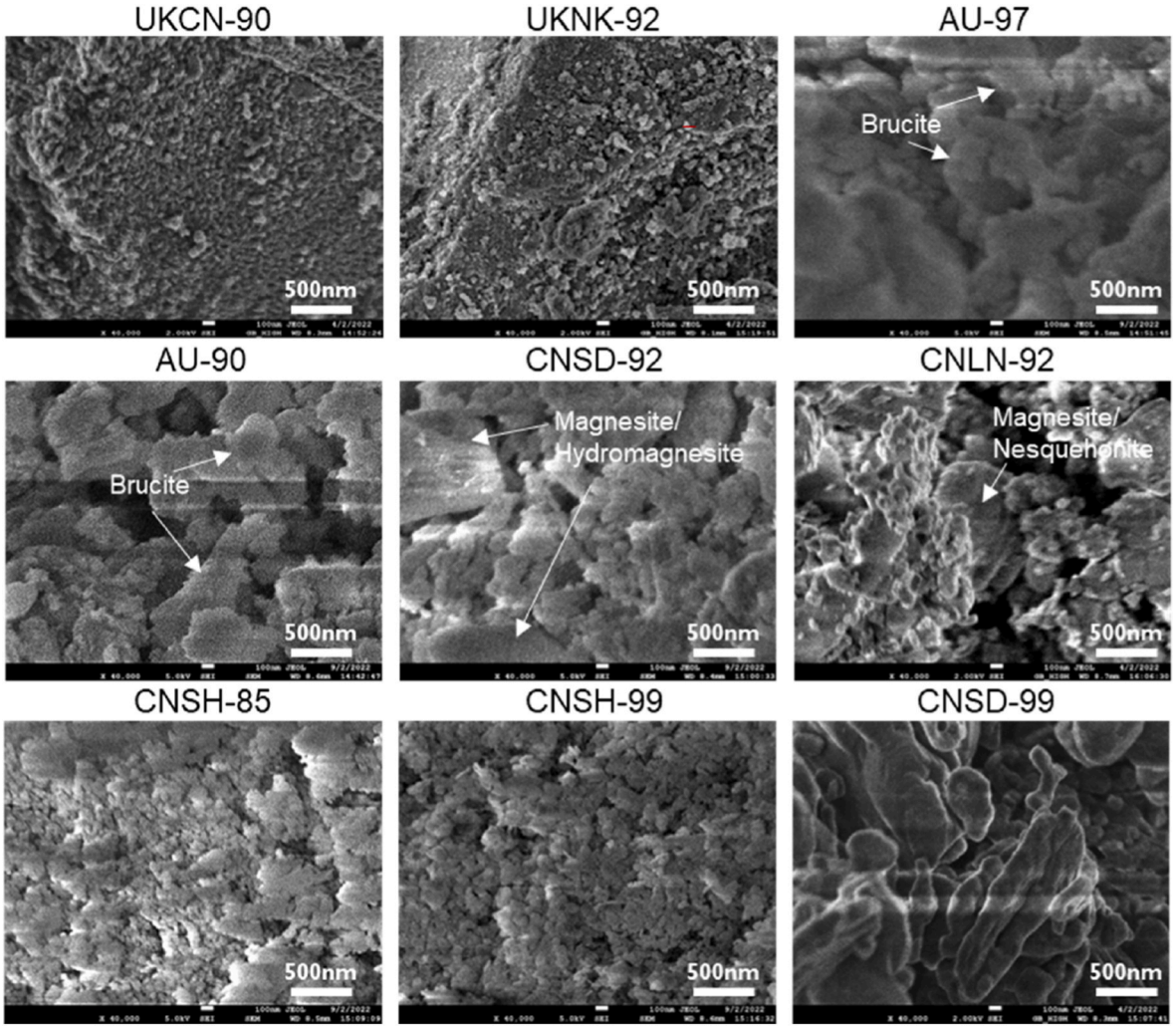

Fig. 8. Microstructures of the nine commercial RMCs.

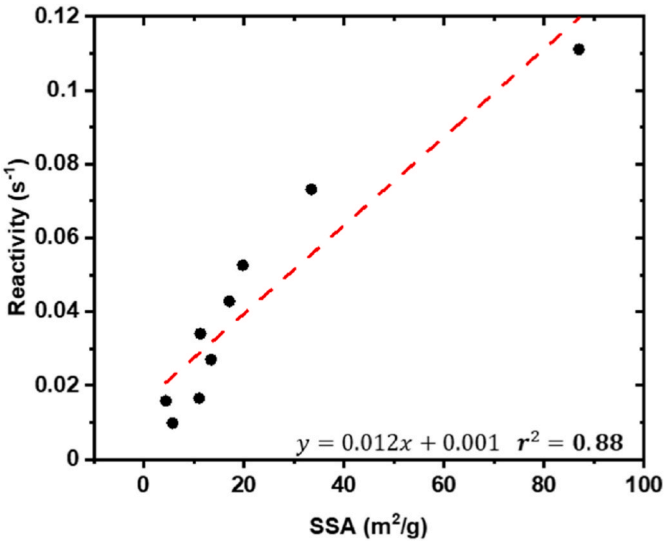

Fig. 9. Relationship between reactivity and SSA.

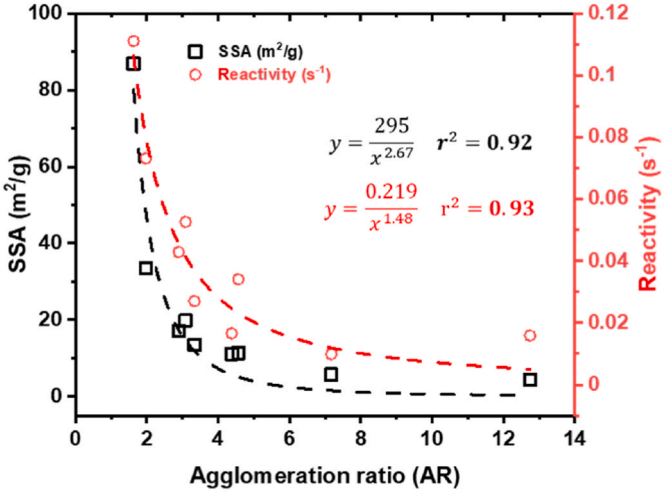

Fig. 10. Relationship between AR and SSA and reactivity.

high $Mg(OH)_2$ and relatively low MgO contents.

Fig. S4 displays a comparison of the cumulative heats of all samples at different stages of hydration. Samples with high reactivities, such as CNSH-85 and CNSH-99, revealed high heat accumulation during the first 6 h; whilst CNLN-92 and CNSD-99 showed limited cumulative heat initially, followed by a major heat release in the second day. All samples indicated lower heat accumulations on the third day than second day, indicating that the hydration rate gradually decreased after 2 days. Notably, AU-90 and AU-97 had the lowest cumulative heat during the first 3 days, which could be attributed to their relatively low MgO purities (Fig. 5). Alternatively, UKCN-90 and UKNK-92 demonstrated a similar cumulative heat after 3 days. Although the latter contained slightly less MgO (Fig. 5), its higher reactivity promoted its hydration during the first 6 h, resulting in a similar accumulative heat at the end of 3 days, in comparison with UKCN-90 (Fig. S4) [43]. For CNSD-99 and CNSH-85, which showed similar purities at ~95% (Fig. 5), their final cumulative heats were comparable, whereas the development of their cumulative heat differed. Accordingly, CNSH-85 released almost half of the heat during the first 6 h, while CNSD-99 mainly released heat after 6 h, linked with the variations in their reactivities [43].

3.3.2. *Strength development*

The compressive strength of RMC concrete specimens subjected to ambient curing for 28 days is presented in Fig. 12. Most samples revealed strengths below 5 MPa, which was due to the limited contribution of hydration to strength development, in line with the findings of previous studies [14,42]. However, CNLN-92 and CNSD-99 samples developed considerably high strengths of 10.7 MPa and 14.2 MPa, respectively, with slightly larger standard deviations, due to the variation of the strength developed in different samples. Considering the low reactivities of these samples, these higher strengths were unexpected. Previous studies reported that the final hydration degree of MgO samples was comparable, independent of their reactivity [45]. In this study, RMC samples with high reactivities exhibited very high initial hydration rates. Considering that the hydration of MgO results in volume expansion [46], the rapid progress of hydration in samples with high reactivities could initially lead to expansion, forming a porous structure and induce cracks, as shown in Fig. 12. Furthermore, the rapid formed reaction products may cover unreacted MgO particles [26], limiting further hydration and strength development. In contrast, samples with lower reactivities, such as CNLN-92 and CNSD-99, represented a constant hydration rate over time, inducing a denser structure.

The strengths of RMC-based concrete specimens subjected to carbonation curing up to 28 days are shown in Fig. 13. Generally, all samples revealed higher strengths than their counterparts cured under ambient conditions due to the formation of HMCs under carbonation conditions [9,17]. CNSD-99 achieved the highest strength at all ages, revealing a maximum strength of ~70 MPa at 7 days. Although CNSD-99 demonstrated a low SSA and reactivity, its strength development was linked with the progress of hydration and carbonation reactions observed in this sample. Accordingly, CNSD-99 showed a linear increase

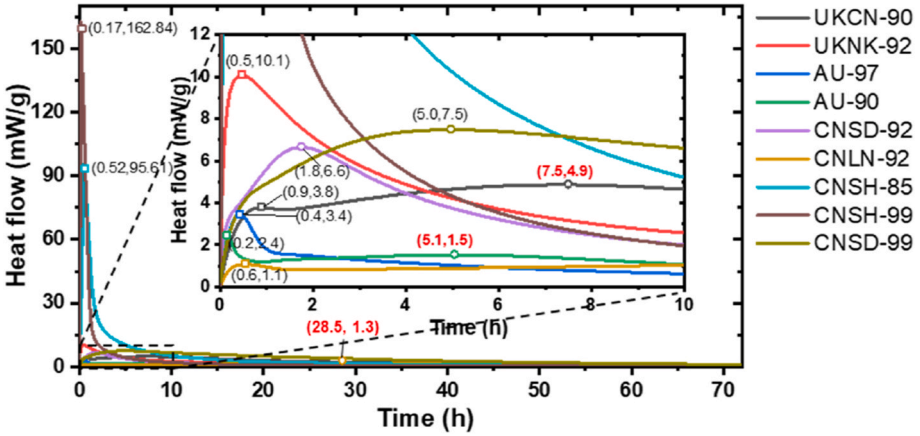

Fig. 11. Heat flow diagrams of the nine commercial RMCs.

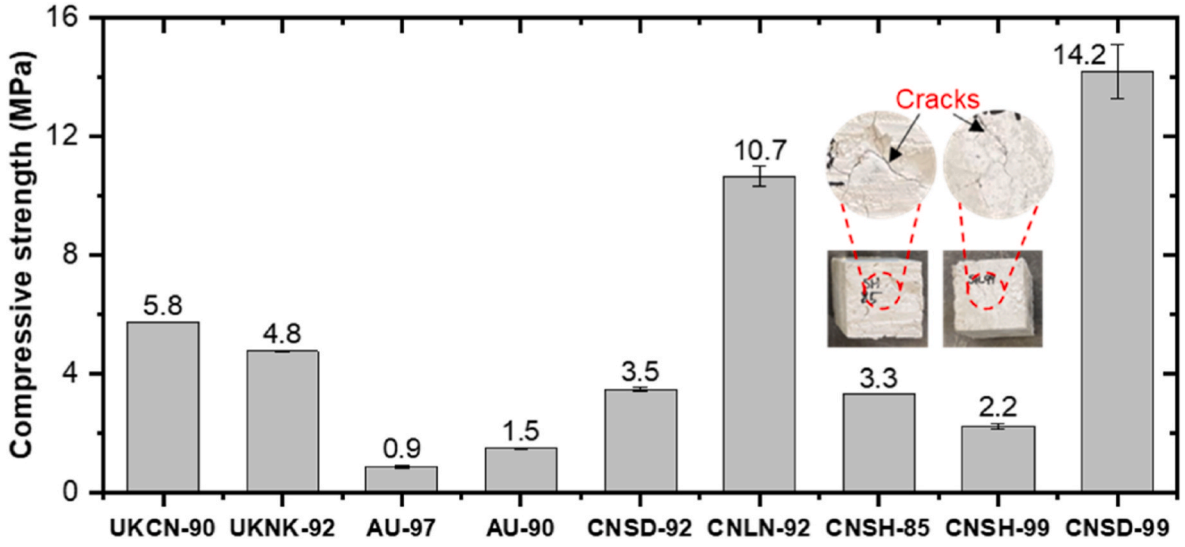

Fig. 12. 28-day compressive strength of RMC concrete samples under ambient curing.

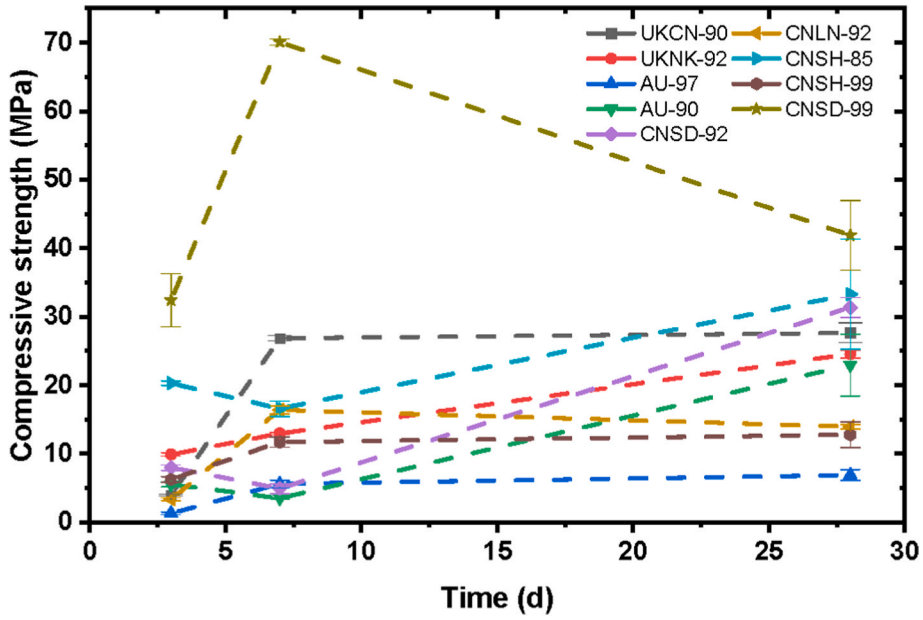

Fig. 13. Compressive strength of RMC concrete samples under carbonation curing.

in cumulative heat and surpassed others until the end of 3 days (Fig. S3). This consistent progress in hydration could reduce rapid volume expansion [46] and thermal cracking [47], resulting in the stable precipitation of $Mg(OH)_2$. As the carbonation of $Mg(OH)_2$ could be more favorable than MgO [48], the constant progress of hydration did not only provide enough $Mg(OH)_2$ for carbonation, but also facilitated a continuous carbonation reaction, thereby resulting in a denser structure [3] and contributing to strength development [15,49]. In contrast, although the more reactive samples such as CNSH-99, produced more $Mg(OH)_2$ at the beginning, the rapid precipitation of reaction products could form a surface layer on unreacted MgO particles, thereby limiting further hydration and carbonation, as well as strength development [9].

Therefore, for a uniform reaction pattern, RMC samples shall be neither too reactive (e.g. CNSH-99) to induce rapid hydration and cracks initially, nor too unreactive (e.g. CNLN-92) to demonstrate limited hydration for strength development. Alternatively, RMC samples with an optimized reactivity (e.g. CNSD-99), which exhibit a constant progress of hydration should be targeted. Such hydration behavior can be considered as a key feature of a promising RMC source.

Three types of strength development trends were identified: (i) Continuous increase; (ii) decrease followed by an increase; and (iii) increase followed by a decrease. Accordingly, UKCN-92, UKNK-90, AU-97 and CNSH-99 samples were in the 1st category, achieving a constant increase in strength over time for up to 28 days, which was in line with most results reported in the literature [14,15,17,50]. AU-90, CNSD-92 and CNSH-85 samples showed a decrease in strength from 3 to 7 days, followed by an increase from 7 to 28 days, corresponding to type (ii). CNLN-92 and CNSD-99 presented an increase in strength from 3 to 7 days and a decrease from 7 to 28 days, corresponding to type (iii), in line with the trend previously reported by Hay and Celik [10]. The variations in strength development trends were essentially related to the differences in the properties of RMCs. For instance, CNLN-92 and CNSD-99, categorized as type (iii), demonstrated the lowest reactivity. Within these samples, the reduction of the strength from 7 to 28 days was attributed to internal hydrostatic pressure induced by the absorption of water for the further hydration of unreacted MgO [10]. However, the

variations in strength development trends corresponding to RMC types (i) and (ii) were more influenced by the combined effects of purity, SSA, reactivity and AR value instead of a simple link to the reactivity. Amongst type (ii), both chemical compositions and reactivities of samples AU-90, CNSD-92 and CNSH-85 varied significantly. Overall, the strengths results demonstrated that concrete specimens made from different RMCs revealed different strength development behaviors, indicating the room for variability in performance, although all samples were categorized as "reactive".

3.4. Correlation between different properties and performance

In this study, the chemical and physical properties, hydration heat and strength development of different commercial RMC samples were investigated and compared. Furthermore, Pearson correlation coefficient was used to establish correlations between different factors. The results are presented in Fig. 14, where IND1-12 represent all the factors considered. All the factors were selected strategically to establish correlations between the properties of RMC samples and their performance. For example, IND5 represents the heat flow at the first peak, revealing the maximum hydration rate that RMC samples can achieve, which is critical for their strength development, especially at early stages. Additionally, IND7 accounts for the accumulative heat during the first 6 h, which plays a key role in revealing hydration kinetics (Fig. S4) and its associated effect (Figs. 12 and 13). The asterisk represents the ones with p values lower than 0.05, indicating a significant difference exists between those two factors [51]. All factors could be divided into three groups, depending on their link with the properties, hydration and strength development of the RMC samples, as labeled in Fig. 14.

In terms of hydration, among IND5-8, IND5 (heat flow at the 1st peak (mW/g)) exhibited a strong positive correlation with IND7 (accumulative heat (6 h) (J/g)). Such correlation is reasonable since the accumulative heat during the first 6 h is highly dependent on the heat flow rate at the 1st peak, which occurred before 6 h for all MgO samples. When the properties (IND1-4) and hydration (IND5-8) (green rectangle) were investigated, IND5 indicated positive correlations with IND2 (reactivity (reciprocal of time, s^{-1})) and IND3 (SSA (m^2/g), which revealed that RMC powders with a greater reactivity and larger SSA could always be expected to result in a higher heat flow rate at the 1st peak. Another significant positive correlation was observed between IND2 and IND7, showing that the reactivity of RMC samples played an important role in the cumulative heat during the first 6 h. In contrary, the cumulative heat up to 3 days was more influenced by the purity and AR of RMC, as revealed by the Pearson coefficients of IND8 against IND1 and IND4. The other element, IND6 (time of the first peak (h)), exhibited non-significant correlations with the other properties of RMC samples.

In terms of strength (IND9-12), the strengths obtained at different ages and curing conditions all displayed positive correlations with each other. In particular, IND9 (strength after 3 d carbonation (MPa)) showed strong positive correlations ($r > 0.8$) with IND10 (strength after 7 d carbonation (MPa)) and IND11 (strength after 28 d carbonation (MPa)), demonstrating that RMC samples with a greater strength after 3 days of carbonation were likely to achieve higher strengths after 7 and 28 days. Additionally, there was a positive correlation between IND10 and IND12 (strength after 28 d hydration (MPa)), revealing that RMC samples that revealed higher strengths after 7 days of carbonation also performed better under ambient curing conditions, during which strength development was purely reliant on hydration.

A comparison of factors associated with hydration (IND5-8) and strength (IND9-12) (red rectangle) revealed only two significant correlations. Accordingly, the relationship of IND8 (accumulative heat (3 d) (J/g)) with IND10 (strength after 7 d carbonation (MPa)) and IND12 (strength after 28 d hydration (MPa)) led to coefficient values of 0.74 and 0.95, respectively. The strong correlation between the IND8 and

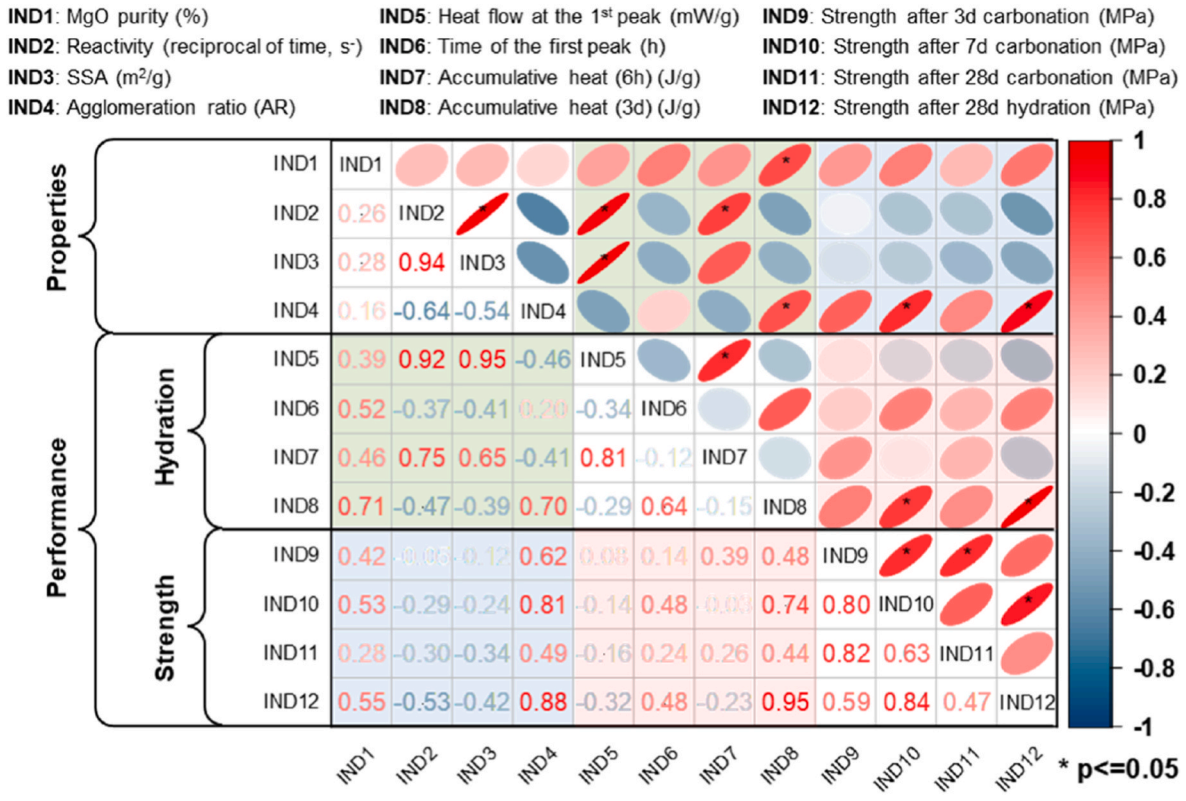

Fig. 14. Pearson correlation coefficient (r) between 12 factors (Colors and ellipses represent strength and direction of the correlation. Asterisks represent significance levels, $p \leq 0.05$. The coefficient values are listed in the lower triangular.). (For interpretation of the references to color in this figure legend, the reader is referred to the Web version of this article.)

IND12 highlighted a clear link between the cumulative heat after 3 days and strength of RMC samples after 28 days of hydration. A comparison of factors associated with RMC properties (IND1-4) and strength (IND9-12) (blue rectangle) revealed large variations in the correlation between different factors, with values ranging from −0.05 to 0.88. Among these factors, only IND4 (agglomeration ratio (AR)) showed significant correlations with IND10 and IND12, indicating the link between AR value and strength of RMC samples after 7 days of carbonation and 28 days of hydration.

Based on the information presented in Fig. 14, the purity and AR showed positive linear correlation with the strength of RMC mixes subjected to different curing conditions, while the reactivity and SSA of RMC demonstrated negative correlations with strength. However, the correlation of AR against the 28-day strength under ambient curing conditions and 7-day strength under carbonation conditions were most significant. Since higher purity of a sample directly corresponds to the amount of MgO available for reaction, it is natural that this component benefits the hydration of RMC and improves strength consequently. However, the positive correlation between AR and strength is rarely discussed, though agglomeration was reported to reduce the reactivity of RMC [13]. It can be seen that RMC powders with high AR values, such as CNLN-92 and CNSD-99, exhibited relatively more stable hydration rates, which regulated the associated volume expansion [46] and thermal cracking due to hydration heat [47]. Alternatively, the hydration degrees of RMC samples were comparable as reactivity did not play a significant role after 28 days [45]. Considering that the strength development of RMC-based samples depends on the hydration and subsequent carbonation of MgO [17,49], limiting volume expansion and thermal cracking throughout this process via the use of RMCs with higher AR values could present benefits.

Another interesting finding was the negative correlation of strength with reactivity and SSA. In general, RMC powders with high reactivities are preferred as a binder as they could react at a faster rate and to a higher degree than those with lower reactivities [52]. This approach does not seem to align with the results presented in this study, especially for the strength developed after 28 days of ambient curing. However, the relatively low correlation coefficients ranging from −0.05 to −0.53 do not present a strong relationship between strength and SSA. Previous studies have shown that hard/dead-burnt MgO with a much lower reactivity exhibited a lower hydration rate than reactive MgO [53], leading to limited strength development [54]. However, when a range of reactive MgO samples were compared amongst each other, those with very high reactivities were reported to potentially cause expansion [46] and form a porous structure. In addition to expansion, a rapid formation of reaction products on the surface layer of unreacted MgO particles can limit further hydration and strength development [26]. A similar phenomenon was reported as a part of the hydration mechanism of tricalcium silicate in PC [55]. Consequently, an “optimum” reactivity, rather than the highest one, should be used for building applications. This outcome is also supported by the cumulative heat results, where the most reactive sample CNSH-99 demonstrated a much lower cumulative heat at 3 days than that of CNSD-99, whilst both samples presented similar purities. It is also worth noting that a lower reactivity RMC could be favored for MgO–SiO_2–H_2O system to avoid the rapid formation of $Mg(OH)_2$ [56].

Generally, the strength of RMC-based samples is mainly linked with the degree of hydration and subsequent carbonation [17,49,57,58]. When compared to carbonation, hydration provides limited strength development under natural conditions, via the reaction shown in Equation (4), which involves the dissolution of MgO, followed by the precipitation of $Mg(OH)_2$ [53]. During the dissolution of MgO, hydration is directly affected by the reaction rate, which in turn, is governed by the purity and reactivity of MgO. However, the formation of a surface-layer over unreacted MgO and the agglomeration of hydration products limit further hydration [9,59]. Consequently, hydration rate is also affected by physical properties including AR and SSA. Therefore, these properties influence the formation of $Mg(OH)_2$, which would subsequently carbonate to provide strength in RMC-based formulations. On the other hand, different reaction rates and physical properties induce various pore structures, which in turn affect the diffusion and penetration of CO_2, and finally impact strength development.

$$MgO + H_2O \rightarrow Mg(OH)_2 \quad (4)$$

The Pearson coefficient values in Fig. 14 can only indicate a linear correlation and provide a general justification of the relationship between two factors only. To integrate all RMC properties and determine their influence on sample performance, a regression analysis was used. The regression models are shown in Equations (5)–(8), which were calculated at a 95% confidence level. To validate the models, the correlation coefficients (R^2) were listed after equations, where the prediction of IND9, IND10 and IND12 was within an acceptable range from 0.76 to 0.99 [60]. However, the prediction of IND11 (strength after 28 days of carbonation) was not straightforward as it did not present a high correlation coefficient ($R^2 = 0.38$). For 3-day and 7-day strengths under carbonation conditions and 28-day strength under natural conditions, strength development was dominated by hydration and RMC properties that determined reaction mechanisms. However, for strength development after 28 days under carbonation conditions, the penetration and dissolution of CO_2 and formation of carbonated products became critical for the mechanical performance of RMC-based samples [61]. In this case, the pore structure and microstructural development of these samples also need to be considered [2].

Based on the proposed equations, both purity and AR of RMC demonstrated a positive correlation with strength developed under natural and carbonation curing. High purities corresponded to higher MgO contents available as a reactant for hydration and subsequent carbonation to contribute to the strength gain [1,62]. Alternatively, strength development under ambient curing showed negative correlations with SSA and positive correlations with reactivity. However, strength developed under carbonation curing was positively correlated to SSA and negatively correlated to reactivity. These variations in the relationship between performance and SSA/reactivity under different curing conditions are an indication of the complicated nature of using RMC as a binder. To simply this process, the linear correlation between SSA and reactivity as established in Section 3.2 (Equation (9)) was employed to simplify Equations (5)–(8) into Equations (10)–(13). It can be seen that the strength developed under carbonation curing is positively correlated to reactivity, which reversed to negative under ambient curing. These variations in the effects of reactivity should be attributed to the different mechanism of strength development of RMC under natural and carbonation curing conditions. It was reported that RMC with an extremely high reactivity could achieve a majority of its hydration within 1 day [4]. The rapid precipitation of the hydration product, $Mg(OH)_2$, forms a surface layer on unreacted particles, preventing further hydration [9,44]. Furthermore, the excessive expansion and possible thermal cracking would potentially limit the strength development of RMC under ambient conditions [46,47].

$$\begin{aligned} IND9 = &-18.18 + 4.25\,IND1 + 513.56\,IND2 - 0.46\,IND3 + 2.99\,IND4 \quad R^2 \\ &= 0.76 \end{aligned} \quad (5)$$

$$\begin{aligned} IND10 = &-27.91 + 20.61\,IND1 + 317.46\,IND2 - 0.27\,IND3 \\ &+ 5.34\,IND4 \quad R^2 \\ &= 0.85 \end{aligned} \quad (6)$$

$$\begin{aligned} IND11 = &8.86 + 8.11\,IND1 + 268.70\,IND2 - 0.38\,IND3 + 1.48\,IND4 \quad R^2 \\ &= 0.38 \end{aligned} \quad (7)$$

$$IND12 = -1.15 + 6.59\ IND1 - 63.90\ IND2 + 0.04\ IND3 + 0.79\ IND4\ R^2 = 0.99 \quad (8)$$

$$IND2 = 0.012\ IND3 + 0.001\ R^2 = 0.88 \quad (9)$$

$$IND9 = -18.18 + 4.25\ IND1 + 5.70\ IND3 + 2.99\ IND4 \quad (10)$$

$$IND10 = -27.91 + 20.61\ IND1 + 3.54\ IND3 + 5.34\ IND4 \quad (11)$$

$$IND11 = 8.86 + 8.11\ IND1 + 2.84\ IND3 + 1.48\ IND4 \quad (12)$$

$$IND12 = -1.15 + 6.59\ IND1 - 0.73\ IND3 + 0.79\ IND4 \quad (13)$$

4. Conclusions

This study presented a detailed characterization of 9 commercially available RMC samples obtained from different sources and production methods, leading to a discussion on mechanical performance. Correlations between the properties of different RMC powders and their strength development under hydration and carbonation conditions were established. Finally, regression models were proposed to predict the strength of RMC-based samples. The main findings are concluded as follows.

- A strong linear correlation was found between the reactivity and SSA, along with an inverse proportionality correlation of AR with reactivity and SSA.
- The heat flow behavior was highly associated with reactivity. A positive correlation between the cumulative heat during the first 6 h and reactivity was revealed, whereas the correlation between cumulative heat during the first 3 days and reactivity was not clear. RMC samples with the highest reactivities led to the highest amount of heat release within the first 6 h, while the least reactive RMC samples demonstrated a relatively constant heat release rate up to 3 days.
- The investigated samples revealed distinct strength development trends that were categorized under 3 groups. The strength values obtained under both ambient and carbonation conditions were all positively correlated with the cumulative heat released during the first three days of hydration.
- Out of all properties, purity and AR both indicated positive correlations with strength. Reactivity of RMC showed a positive correlation with strength under carbonation conditions and a negative correlation under ambient curing conditions.

Overall, the outcome of this work has presented clear links with the properties of different RMC powders and their mechanical performance as a binder. It was concluded that reactivity should not be regarded as the only critical parameter involved in the decision-making process when determining the suitability of RMC as a binder. Other properties such as purity, SSA and AR, also play key roles in strength development. To incorporate the effects of all these properties, the models proposed in this study can be used as a guideline for researchers and practitioners, who are interested in using RMC as a binder.

Credit author statement

T. Mi: Conceptualization, Methodology, Formal analysis, Writing - Original Draft. **E.H. Yang**: Conceptualization, Methodology, Writing - Review & Editing, Supervision. **C. Unluer**: Conceptualization, Methodology, Writing - Review & Editing, Supervision.

Declaration of competing interest

The authors declare that they have no known competing financial interests or personal relationships that could have appeared to influence the work reported in this paper.

Data availability

No data was used for the research described in the article.

Acknowledgements

The authors would like to acknowledge financial support from the Ministry of National Development, Singapore (CoT-V1-2020-1).

Appendix A. Supplementary data

Supplementary data to this article can be found online at https://doi.org/10.1016/j.cemconcomp.2023.104984.

References

[1] N.T. Dung, C. Unluer, Performance of reactive MgO concrete under increased CO2 dissolution, Cement Concr. Res. 118 (2019) 92–101.
[2] C. Unluer, A. Al-Tabbaa, Enhancing the carbonation of MgO cement porous blocks through improved curing conditions, Cement Concr. Res. 59 (2014) 55–65.
[3] L. Mo, D.K. Panesar, Accelerated carbonation – a potential approach to sequester CO2 in cement paste containing slag and reactive MgO, Cem. Concr. Compos. 43 (2013) 69–77.
[4] F. Jin, A. Al-Tabbaa, Characterisation of different commercial reactive magnesia, Adv. Cement Res. 26 (2014) 101–113.
[5] V. Birchal, S. Rocha, V. Ciminelli, The effect of magnesite calcination conditions on magnesia hydration, Miner. Eng. 13 (2000) 1629–1633.
[6] L. Mo, M. Deng, M. Tang, Effects of calcination condition on expansion property of MgO-type expansive agent used in cement-based materials, Cement Concr. Res. 40 (2010) 437–446.
[7] C.K. Chau, Z. Li, Accelerated reactivity assessment of light burnt magnesium oxide, J. Am. Ceram. Soc. 91 (2008) 1640–1645.
[8] M.A. Shand, F. Jin, 0 - introduction – characterization of MgO, in: Mark Alexander Shand, et al. (Eds.), Magnesia Cements, 2020. Oxford.
[9] N.T. Dung, C. Unluer, Advances in the hydration of reactive MgO cement blends incorporating different magnesium carbonates, Construct. Build. Mater. 294 (2021), 123573.
[10] R. Hay, K. Celik, Hydration, carbonation, strength development and corrosion resistance of reactive MgO cement-based composites, Cement Concr. Res. 128 (2020), 105941.
[11] G. Smithson, N. Bakhshi, The kinetics and mechanism of the hydration of magnesium oxide in a batch reactor, Can. J. Chem. Eng. 47 (1969) 508–513.
[12] P. Hewlett, Lea's Chemistry of Cement and Concrete, 5, Elsevier Science, 2019.
[13] G. Gravogl, C. Knoll, J.M. Welch, W. Artner, N. Freiberger, R. Nilica, E. Eitenberger, G. Friedbacher, M. Harasek, A. Werner, Cycle stability and hydration behavior of magnesium oxide and its dependence on the precursor-related particle morphology, Nanomaterials 8 (2018) 795.
[14] S. Ma, A.H. Akca, D. Esposito, S. Kawashima, Influence of aqueous carbonate species on hydration and carbonation of reactive MgO cement, J. CO2 Util. 41 (2020), 101260.
[15] N.T. Dung, C. Unluer, Sequestration of CO2 in reactive MgO cement-based mixes with enhanced hydration mechanisms, Construct. Build. Mater. 143 (2017) 71–82.
[16] L. Wang, L. Chen, J.L. Provis, D.C.W. Tsang, C.S. Poon, Accelerated carbonation of reactive MgO and Portland cement blends under flowing CO2 gas, Cem. Concr. Compos. 106 (2020), 103489.
[17] S. Ruan, C. Unluer, Influence of mix design on the carbonation, mechanical properties and microstructure of reactive MgO cement-based concrete, Cem. Concr. Compos. 80 (2017) 104–114.
[18] S. Ruan, E.-H. Yang, C. Unluer, Production of reactive magnesia from desalination reject brine and its use as a binder, J. CO2 Util. 44 (2021), 101383.
[19] T. Hoang, N.T. Dung, C. Unluer, J. Chu, Use of microbial carbonation process to enable self-carbonation of reactive MgO cement mixes, Cement Concr. Res. 143 (2021), 106391.
[20] G. Le Saoût, V. Kocaba, K.J.C. Scrivener, c. research, Application of the Rietveld Method to the Analysis of Anhydrous Cement, 41, 2011, pp. 133–148.
[21] K. Itatani, A. Itoh, F. Howell, A. Kishioka, M. Kinoshita, Densification and microstructure development during the sintering of submicrometers magnesium oxide particles prepared by a vapour-phase oxidation process, J. Mater. Sci. 28 (1993) 719–728.
[22] ASTM, C1702 Standard Test Method for Measurement of Heat of Hydration of Hydraulic Cementitious Materials Using Isothermal Conduction Calorimetry, ASTM International, 2015.

[23] ASTM C109/C109M (2016) Standard Test Method for Compressive Strength of Hydraulic Cement Mortars (Using 2-in. or [50-mm] Cube Specimens). ASTM International, West Conshohocken, PA. https://www.astm.org.
[24] B. Panda, C. Sonat, E.-H. Yang, M.J. Tan, C. Unluer, Use of magnesium-silicate-hydrate (M-S-H) cement mixes in 3D printing applications, Cem. Concr. Compos. 117 (2021), 103901.
[25] N.T. Dung, A. Lesimple, R. Hay, K. Celik, C. Unluer, Formation of carbonate phases and their effect on the performance of reactive MgO cement formulations, Cement Concr. Res. 125 (2019), 105894.
[26] C. Kuenzel, F. Zhang, V. Ferrándiz-Mas, C.R. Cheeseman, E.M. Gartner, The mechanism of hydration of MgO-hydromagnesite blends, Cement Concr. Res. 103 (2018) 123–129.
[27] J. Zhu, N. Ye, J. Liu, J. Yang, Evaluation on hydration reactivity of reactive magnesium oxide prepared by calcining magnesite at lower temperatures, Ind. Eng. Chem. Res. 52 (2013) 6430–6437.
[28] G. Balakrishnan, R. Velavan, K. Mujasam Batoo, E.H. Raslan, Microstructure, optical and photocatalytic properties of MgO nanoparticles, Results Phys. 16 (2020), 103013.
[29] Frantina, Y. I., Fajaroh, F., Nazriati, Yahmin & Sumari. in AIP Conference *Proceedings*. 070003 (AIP Publishing LLC).
[30] R. Hay, N.T. Dung, A. Lesimple, C. Unluer, K. Celik, Mechanical and microstructural changes in reactive magnesium oxide cement-based concrete mixes subjected to high temperatures, Cem. Concr. Compos. 118 (2021), 103955.
[31] G. Giester, C. Lengauer, B.J. Rieck, The crystal structure of nesquehonite, MgCO3·3H2O, from Lavrion, Greece, Mineral Petrol. 70 (2000) 153–163.
[32] F.P. Glasser, G. Jauffret, J. Morrison, J.-L. Galvez-Martos, N. Patterson, M. Imbabi, Sequestering CO2 by mineralization into useful nesquehonite-based products, Front. Energy Res. 4 (2016), 3.
[33] M.-H. Lee, D.-G. Park, Preparation of MgO with high surface area, and modification of its pore characteristics, Bull. Kor. Chem. Soc. 24 (2003) 1437–1443.
[34] N. José, H. Ahmed, B. Miguel, E. Luís, d.B. Jorge, Magnesia (MgO) production and characterization, and its influence on the performance of cementitious materials: a review, Materials 13 (2020) 4752.
[35] B. Wang, W. Zhang, W. Zhang, C. Yu, G. Wang, L. Huang, A. Mujumdar, Influence of drying processes on agglomeration and grain diameters of magnesium oxide nanoparticles, Dry. Technol. 25 (2007) 715–721.
[36] L. Kirkes, Y. Xiong, Solution Chemistry:Advances in Research and Applications Chapter 2. Experimental Determination of Brucite Solubility in NaCl Solutions at Elevated Temperatures, 2018, pp. 47–68.
[37] L. Kumari, W. Li, C.H. Vannoy, R.M. Leblanc, D. Wang, Synthesis, characterization and optical properties of magnesium hydroxide micro-/nanostructures, APS March Meeting Abstracts (2009) 142.
[38] S. Kumar, E.-H. Yang, C. Unluer, Investigation of chloride penetration in carbonated reactive magnesia cement mixes exposed to cyclic wetting–drying, Construct. Build. Mater. 284 (2021), 122837.
[39] N. Raza, Z.I. Zafar, M. Najam-ul-Haq, Utilization of formic acid solutions in leaching reaction kinetics of natural magnesite ores, Hydrometallurgy 149 (2014) 183–188.
[40] J.I. Goldstein, D.E. Newbury, P. Echlin, D.C. Joy, A. Romig, C.E. Lyman, C. Fiori, E. Lifshin, J.I. Goldstein, D.E. Newbury, X-ray microanalysis: a text for biologists, M. S. & geologists. Coating and conductivity techniques for SEM and microanalysis, Scanning Electron. Microsc. X-Ray. Microanal. (1992) 671–740.
[41] R. Hay, B. Peng, K. Celik, Filler effects of CaCO3 polymorphs derived from limestone and seashell on hydration and carbonation of reactive magnesium oxide (MgO) cement (RMC), Cement Concr. Res. 164 (2023), 107040.
[42] N.T. Dung, C. Unluer, Improving the performance of reactive MgO cement-based concrete mixes, Construct. Build. Mater. 126 (2016) 747–758.
[43] L. Huang, Z. Yang, S. Wang, Influence of calcination temperature on the structure and hydration of MgO, Construct. Build. Mater. 262 (2020), 120776.
[44] L. Szymoniak, D. Claveau-Mallet, M. Haddad, B. Barbeau, Application of magnesium oxide media for remineralization and removal of divalent metals in drinking water treatment: a review, Water 14 (2022) 633.
[45] M. Aphane, E. Van Der Merwe, C. Strydom, calorimetry, Influence of hydration time on the hydration of MgO in water and in a magnesium acetate solution, J. Therm. Anal. 96 (2009) 987–992.
[46] L. Mo, M. Deng, M. Tang, A. Al-Tabbaa, MgO expansive cement and concrete in China: past, present and future, Cement Concr. Res. 57 (2014) 1–12.
[47] I. Chu, Y. Lee, M.N. Amin, B.-S. Jang, J.-K. Kim, Application of a thermal stress device for the prediction of stresses due to hydration heat in mass concrete structure, Construct. Build. Mater. 45 (2013) 192–198.
[48] J. Fagerlund, R. Zevenhoven, An experimental study of Mg(OH)2 carbonation, Int. J. Greenh. Gas Control 5 (2011) 1406–1412.
[49] C. Unluer, A. Al-Tabbaa, Impact of hydrated magnesium carbonate additives on the carbonation of reactive MgO cements, Cement Concr. Res. 54 (2013) 87–97.
[50] X. Li, R. Qiu, F. Xue, L. Fang, F. Cheng, Effects of unreactive MgO and impurities in light burned MgO on the hydration process and performance of base magnesium sulfate cement, Construct. Build. Mater. 240 (2020), 117854.
[51] S. Greenland, S.J. Senn, K.J. Rothman, J.B. Carlin, C. Poole, S.N. Goodman, D. G. Altman, Statistical tests, P values, confidence intervals, and power: a guide to misinterpretations, Eur. J. Epidemiol. 31 (2016) 337–350.
[52] H. Dong, C. Unluer, E.-H. Yang, A. Al-Tabbaa, Recovery of reactive MgO from reject brine via the addition of NaOH, Desalination 429 (2018) 88–95.
[53] J.J. Thomas, S. Musso, I. Prestini, Kinetics and activation energy of magnesium oxide hydration, J. Am. Ceram. Soc. 97 (2014) 275–282.
[54] P.K. Mehta, History and status of performance tests for evaluation of soundness of cements. Cement Standards-Evolution and Trends, ASTM International, 1978.
[55] J. Beaudoin, I. Odler, 5 - hydration, setting and hardening of portland cement, in: Peter C. Hewlett, Liska Martin (Eds.), Lea's Chemistry of Cement and Concrete, fifth ed., 2019.
[56] Z. Li, Y. Xu, T. Zhang, J. Hu, J. Wei, Q. Yu, Effect of MgO calcination temperature on the reaction products and kinetics of MgO–SiO2–H2O system, J. Am. Ceram. Soc. 102 (2019) 3269–3285.
[57] L. Vandeperre, M. Liska, A. Al-Tabbaa, Hydration and mechanical properties of magnesia, pulverized fuel ash, and portland cement blends, J. Mater. Civ. Eng. 20 (2008) 375–383.
[58] L. Mo, D.K. Panesar, Effects of accelerated carbonation on the microstructure of Portland cement pastes containing reactive MgO, Cement Concr. Res. 42 (2012) 769–777.
[59] Z. Xing, L. Bai, Y. Ma, D. Wang, M. Li, Mechanism of magnesium oxide hydration based on the multi-rate model, Materials 11 (2018) 1835.
[60] U. Atici, Prediction of the strength of mineral admixture concrete using multivariable regression analysis and an artificial neural network, Expert Syst. Appl. 38 (2011) 9609–9618.
[61] S. Ruan, C. Unluer, Influence of supplementary cementitious materials on the performance and environmental impacts of reactive magnesia cement concrete, J. Clean. Prod. 159 (2017) 62–73.
[62] N.T. Dung, R. Hay, A. Lesimple, K. Celik, C. Unluer, Influence of CO2 concentration on the performance of MgO cement mixes, Cem. Concr. Compos. 115 (2021), 103826.